Islamic Azad University

Journal of

Optoelectronical Nanostructures

Volume 11, Issue 1, Winter 2021, Page 1-101

PResearch Paper

Orientation-Dependent Thermoelectric Engineering of Rectangular Nanopores in Bismuth Nanoribbons: Effects on Electronic Conductance, Bandgap, and Seebeck Coefficient

Hossein Karbaschi*[,1], Mohammad Saiid Sobhan[2], Nafise Nouri[3]

[1] Faculty of Science, Mahallat Institute of Higher Education, Mahallat, 37811-51958, Iran
[2] Faculty of Engineering, Mahallat Institute of Higher Education, Mahallat, 37811-51958, Iran
[3] Department of Physics, University of Isfahan, Isfahan 81746-73441, Iran

Received:
Revised:
Accepted:
Published:

Use your device to scan and read the article online

Keywords:
Bismuth,
Electrical Conductance
Nanopore,
Nanoribbons,
Tight-binding.

Abstract:
We investigate the influence of rectangular nanopores on the electronic and thermoelectric properties of zigzag bismuth nanoribbons using a tight-binding framework combined with the Green's function formalism. The study focuses on how the geometry and orientation of nanopores affect the electronic conductance, energy bandgap, and Seebeck coefficient. Our calculations show that introducing nanopores along both the transport and transverse directions strongly modify the transport behavior of the nanoribbon. Elongating the nanopore along the transport direction induces moderate scattering and weak perturbation of conductance, resulting in a slight reduction in transmission and a small widening of the energy gap. In contrast, widening the pore perpendicular to the transport direction produces a much stronger effect, notably suppressing conductance near the Fermi level and significantly increasing the bandgap. Moreover, the

Citation: Hossein Karbaschi, Mohammad Saiid Sobhan, Nafise Nouri. Orientation-Dependent Engineering of Rectangular Nanopores in Bismuth Nanoribbons: Effects on Conductance and Energy Bandgap. **Journal of Optoelectronical Nanostructures.** 2025; 11 (1): 1-12.

***Corresponding author:** Hossein Karbaschi
Address: Faculty of Science, Mahallat Institute of Higher Education, Mahallat, 37811-51958, Iran
Email: h.karbaschi@gmail.com
DOI:

calculated Seebeck coefficient exhibits a remarkable enhancement with increasing pore width, which is attributed to the evolution of the conductance spectrum toward a boxcar-like shape—a feature known to improve thermoelectric performance. These findings demonstrate that nanopore geometry and orientation can be effectively utilized to tailor both the electronic and thermoelectric characteristics of bismuth-based low-dimensional nanostructures for future energy-conversion and nanoelectronic applications.

1. INTRODUCTION

Thermoelectric technology converts waste heat into electrical energy, with applications in industries, vehicles, and devices. It operates on the thermoelectric effect, generating current from temperature differences. Utilizing waste heat sources, it aims to be a sustainable solution, but faces challenges like low efficiency. Recently, many theoretical and experimental efforts have been made to enhance thermoelectric efficiency of energy harvesting applications [1-3].

Low-dimensional materials such as nanoribbons have attracted significant attention due to their unique electronic properties, which are highly sensitive to structural modifications and defects [4-5]. Among them, zigzag bismuth nanoribbons (ZBiNRs) exhibit prominent edge states that strongly influence both conductance and band gap, making them promising candidates for nanoscale electronic and thermoelectric devices. Defect engineering, particularly through the introduction of nanopores [6–9], edge modifications [10,11], and substitutional defects [12–15], has emerged as an effective strategy to tailor the electronic and thermoelectric response of nanoribbons. Previous studies on graphene, phosphorene, and other two-dimensional materials have demonstrated that the size, shape, and type of defects can substantially modify transport properties, energy spectra, and thermoelectric performance. Recent investigations have explored various aspects of bismuth nanoribbons, including their thermoelectric and electronic transport characteristics under different conditions [16–18]. For instance, theoretical studies have shown that zigzag monolayer bismuth nanoribbons with properly tuned on-site potentials can achieve high thermoelectric efficiency and significant power generation [12]. Moreover, the presence of random impurities has been found to affect both conductance and the localization of edge states, highlighting the sensitivity of ZBiNRs to structural disorder. However such a strategy leads to improvement in thermoelectric performance, but the results may change with different configuration of impurities. Also, it has been shown that the strategy of current work leads to a stronger change in electrical conductance and the separation of edge and bulk states [15].

In this work, we employ a tight-binding framework combined with the Green's function formalism to systematically study the orientation-dependent effects of rectangular nanopores on both the electronic conductance, energy bandgap, and Seebeck coefficient of zigzag bismuth nanoribbons. By varying the nanopore geometry along both the transport and transverse directions, we provide

comprehensive insights into how defect engineering can be exploited to tune the electronic and thermoelectric properties of bismuth-based nanostructures for future nanoscale device applications.

2. Model and System Description

Two-dimensional (2D) bismuth (Bi) can be described as a honeycomb lattice composed of two nonequivalent atomic sites, denoted as A and B, as shown schematically in Fig. 1(a). The hexagonal unit cell forms the basis of a buckled honeycomb geometry, in which the two sublattices are vertically displaced with respect to each other, as illustrated in Fig. 1(b). This buckled configuration distinguishes Bi from planar 2D materials such as graphene and originates from the relatively large atomic size of bismuth atoms.

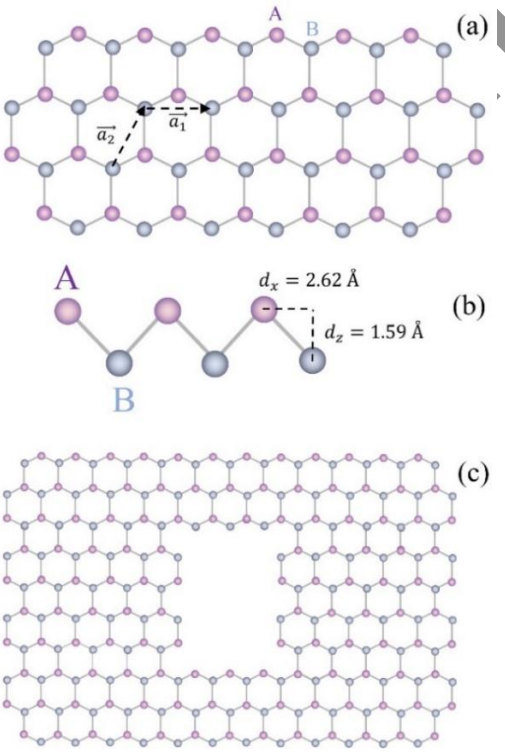

Fig. 1. (a) Top view of the two-dimensional bismuth (Bi) crystal structure with a hexagonal unit cell containing two nonequivalent atoms, labeled A and B. (b) Side view of the freestanding Bi layer showing its buckled honeycomb configuration. (c) Schematic illustration of the studied zigzag Bi nanoribbon with a rectangular nanopore created at the center.

The non-planar structure enhances the stability of the freestanding Bi layer [19] and allows for tunable electronic properties through external factors such as strain[20,21], electric field [22,23], or edge modification [12,17,24,25]. In this work, we consider such a buckled honeycomb lattice as the fundamental structure for constructing zigzag Bi nanoribbons, where edge states and finite-size effects play a crucial role in determining the overall transport characteristics.
As shown in Fig. 1(c), the system under investigation is a zigzag bismuth nanoribbon in which a rectangular nanopore is introduced at the center of the ribbon. To systematically study its impact on the electronic transport characteristics, the nanopore is extended once along the ribbon length and once along its width. These two configurations enable a comparative analysis of how the pore orientation affects the conductance spectrum and the band gap of the nanoribbon.

3. TIGHT-BINDING AND GREEN'S FUNCTION APPROACH

In order to describe the electronic and transport properties of the studied system, we employ the tight-binding (TB) model together with the Green's function formalism [7]. The tight-binding approach provides a convenient and physically intuitive framework to construct the Hamiltonian of a low-dimensional system based on atomic orbitals and hopping interactions between neighboring atoms. In this method, the total energy of electrons is represented as the sum of on-site energies and hopping terms connecting adjacent atoms [12, 26]. The tight-binding parameters used in this work is provided in Tab. 1. This allows us to capture the essential features of the band structure and electronic states of the nanoribbon with relatively low computational cost, while still retaining sufficient accuracy to study quantum transport phenomena.

Spin–orbit coupling (SOC) is not considered in this analysis. This choice was made because, in theoretical models, it can be permissible to simplify the model by neglecting spin–orbit coupling if the focus is solely on non-magnetic electronic properties. The effect of SOC can be added later as a perturbation [15].

The Green's function technique is then applied to obtain information about the propagation of electronic states through the system and to evaluate how electrons are transmitted or reflected at different energy levels. In particular, the Green's function connects the properties of the central device region to those of the left and right leads, enabling the calculation of transmission probabilities.

Table 1. The tight-binding parameters including the on-site energies and the hopping parameters of bulk Bismuth (eV). The superscripts "1" and "2" denote the nearest neighbors and the next nearest neighbors hopping parameters.

Parameters	Magnitude (eV)
E_s	-10.906
E_p	-0.486
$V^1_{ss\sigma}$	-0.608
$V^1_{sp\sigma}$	1.320
$V^1_{pp\sigma}$	1.854
$V^1_{pp\pi}$	-0.600
$V^2_{pp\sigma}$	0.156

In the framework of quantum transport theory, the electronic transmission probability through a nanostructure can be obtained using the Landauer–Büttiker approach combined with the Green's function formalism. The transmission function $T(E)$, which determines the probability that an electron with energy E passes from the left to the right electrode, is calculated as [27]:

$$T(E) = Tr[\Gamma_L G^{ret} \Gamma_R G^{adv}] \quad (1)$$

where Γ_L and Γ_R are the broadening matrices of the left and right electrodes, and G^{ret} and G^{adv} are the retarded and advanced Green's functions of the central scattering region, respectively. The broadening matrices are defined by:

$$\Gamma_{(L,R)} = i(\Sigma^{ret}_{(L,R)} - \Sigma^{adv}_{(L,R)}) \quad (2)$$

where $\Sigma^{ret}_{(L,R)}$ and $\Sigma^{adv}_{(L,R)}$ represent the retarded and advanced self-energy terms describing the coupling between the device and the electrodes. The retarded Green's function of the system is given by:

$$G^{ret}(E) = [E\,I - H - \Sigma^{ret}_L - \Sigma^{ret}_R]^{-1} \quad (3)$$

Here, H denotes the Hamiltonian matrix of the central region, I is the identity matrix, and E is the electron energy.

In this work, all numerical simulations are performed using the Kwant Python package [28], which provides an efficient and flexible platform for modeling quantum transport in tight-binding systems.

4. THERMOELECTRIC EFFECT

The Seebeck coefficient, also known as the thermoelectric sensitivity, represents the magnitude of the induced thermoelectric voltage generated in response to a temperature difference across a material, as described by the Seebeck effect. It characterizes the ability of charge carriers to convert thermal energy into electrical potential and serves as a key parameter in evaluating the thermoelectric behavior of low-dimensional systems. A large Seebeck coefficient indicates that the system can efficiently generate an electric voltage under a small thermal difference.

When a temperature difference (ΔT) is applied between two terminals of a nanoribbon, an open-circuit voltage (ΔV) develops, and the Seebeck coefficient is defined as [27]:

$$S = \frac{\Delta V}{\Delta T}\Big|_{I=0} \tag{4}$$

Within the Landauer–Büttiker and Green's function framework, the Seebeck coefficient can be obtained from the energy-dependent transmission function $T(E)$ through the following relations:

$$L_n = \int (E - \mu)^n T(E) \left(\frac{-\partial f}{\partial E}\right) dE, \tag{5}$$

where $f(E, \mu, T)$ is the Fermi–Dirac distribution function and μ is the chemical potential. The electrical conductance G and Seebeck coefficient S are then expressed as:

$$G = \left(\frac{2e^2}{h}\right) L_0, \tag{6}$$

$$S = -(1/eT) \left(\frac{L_1}{L_0}\right). \tag{7}$$

These relations indicate that the Seebeck coefficient depends on the energy-dependent transport characteristics around the Fermi level. When the transmission spectrum becomes more asymmetric with respect to the chemical potential, the magnitude of S increases. In the present work, the calculated results show that widening the nanopore perpendicular to the transport direction leads to a remarkable improvement in the Seebeck coefficient, confirming that nanopore geometry can effectively enhance the thermoelectric response of zigzag bismuth nanoribbons.

5. RESULTS AND DISCUSSION

The considered system is a zigzag bismuth nanoribbon attached to a cold lead that is kept at room temperature (300 K), and a hot lead, which is 10 degrees warmer than the cold lead. To ensure that the scattering between the wave functions of the edge states does not occur, the width of the nanoribbon is set at 40 atomic rows.

Figure 2 illustrates the variation of the electronic conductance as a function of energy for several nanoribbon configurations with different pore lengths. Here, the width of pore is fixed at 8 atoms. The first row shows the pore with 5 atom length, and the subsequent rows represent lengths of 9, 13, and 17 atoms.

The right panels display the atomic structures of the systems, where the pore is gradually elongated along the transport direction, while the left panels show the corresponding conductance spectra. The conductance is expressed in units of e^2/h.

In all cases, the conductance spectra are nearly symmetric with respect to the Fermi level ($E = 0$), reflecting the approximate electron–hole symmetry of the system. A noticeable suppression of conductance appears around zero energy, indicating the presence of an energy region with reduced transmission probability. This feature suggests that the carriers experience moderate scattering near the Fermi level, resulting in a transport-gap-like behavior.

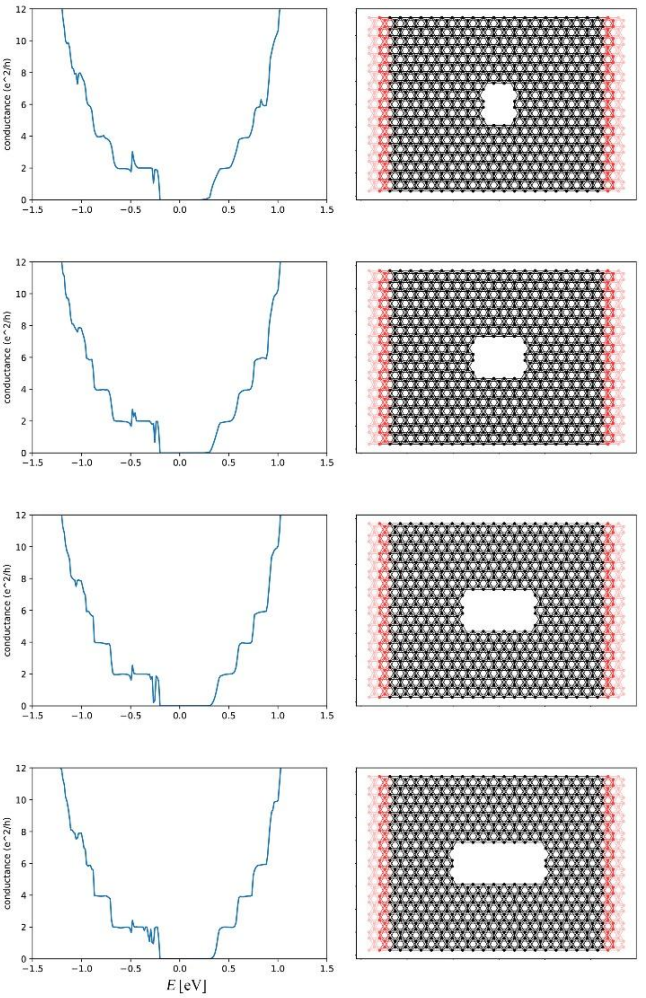

Fig. 2. Electronic conductance spectra of zigzag bismuth nanoribbons with rectangular pores of increasing length. The width of pore is fixed at 8 atoms. The first row shows the pore with 5 atom length, and the subsequent rows represent lengths of 9, 13, and 17 atoms. The atomic configurations on the right illustrate the gradual elongation of the pore along the transport direction, while the corresponding conductance $G(E)$, expressed in units of e^2/h, is shown on the left.

As the pore length increases, a slight but consistent decrease in the overall conductance can be observed across the entire energy range. The quantized steps in the conductance become somewhat smoother, and small oscillations appear in

the transmission curves. These variations imply that elongating the pore introduces additional scattering and interference effects within the nanoribbon, though their overall impact on conductance remains modest.

For low-energy carriers, the influence of pore elongation is more noticeable. Increasing the pore length or removing a larger number of atoms slightly disturbs the conduction pathways and weakens the coherent propagation of electrons through the central region. Consequently, the mean transmission probability decreases marginally, and the conductance around the Fermi level shows a mild reduction. In other words, the elongated pore acts as a weak potential barrier for low-energy electrons, leading to partial reflection and a small decrease in transmission.

In the low-energy range between approximately -0.5eV and -0.2eV, the conductance is mainly governed by the edge-related states of the nanoribbon. When a pore is introduced, new edge boundaries are formed along its upper and lower sides, giving rise to localized electronic states around the pore region. As the pore size increases, the area of these internal edges expands, and the corresponding localized states become more pronounced.

The emergence of these localized edge states around the pore leads to a moderate interaction with the intrinsic edge states of the nanoribbon. This coupling results in a slight distortion of the step-like behavior observed in the conductance spectra. Specifically, the conductance plateaus that correspond to well-defined edge channels become mildly irregular, reflecting the interference between the extended and localized states.

With further elongation of the pore, the localized states around its edges are somewhat strengthened, enhancing their weak hybridization with the nanoribbon's conductive channels. This interaction modestly increases the scattering of low-energy carriers and gradually disrupts the ideal quantization of conductance. Therefore, the observed deviation from a perfect stepwise conductance pattern can be attributed to the increasing, yet moderate, coupling between localized states at the pore edges and the conducting states of the pristine ribbon.

According to the Figure 3, as the pore width increases, a more pronounced decrease in the overall conductance is observed, particularly in the low-energy region near the Fermi level. The quantized steps in the conductance spectra exhibit significant smoothing and degradation, indicating a stronger disruption of the coherent transport channels. The oscillations and irregularities in the transmission curves become more evident, suggesting that widening the pore substantially enhances scattering and quantum interference effects within the nanoribbon.

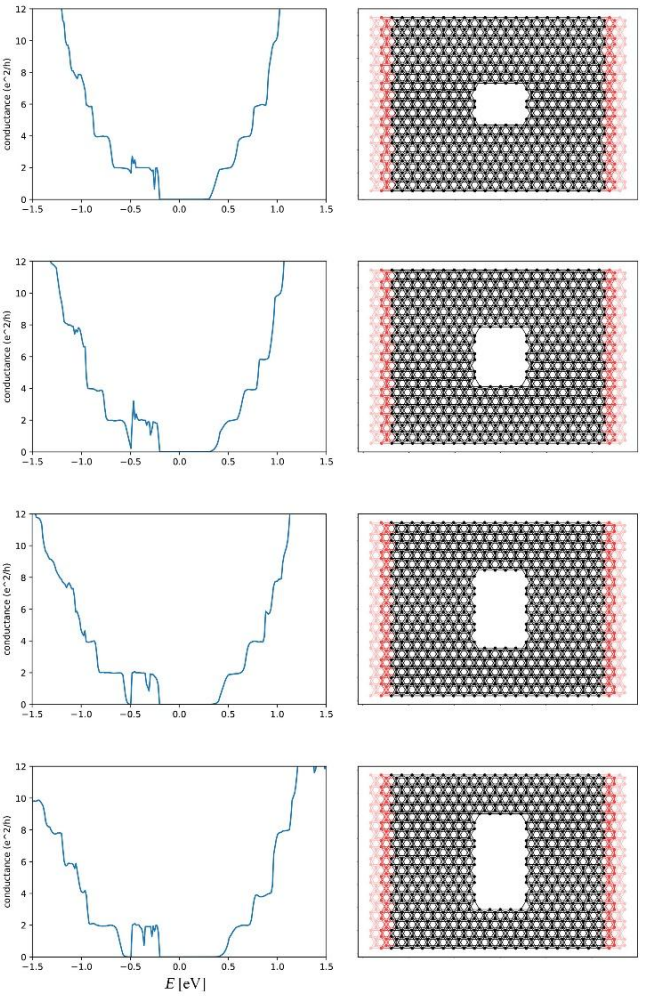

Fig. 3. Electronic conductance spectra of zigzag bismuth nanoribbons with rectangular pores of increasing width. The length of pore is fixed at 9 atoms. The first row shows the pore with 8 atom width, and the subsequent rows represent widths of 12, 16, and 20 atoms. The atomic configurations on the right illustrate the gradual widening of the pore perpendicular to the transport direction, while the corresponding conductance $G(E)$, expressed in units of e^2/h, is shown on the left.

For low-energy carriers, the influence of pore widening is considerably more severe than elongation. As the pore width increases perpendicular to the transport direction, the effective channel width through which electrons can propagate is

reduced. This geometric constriction forces the carriers to travel through narrower conducting pathways on either side of the pore, leading to increased backscattering and reduced transmission probability. Consequently, the conductance around the Fermi level shows a more substantial reduction compared to pore elongation scenarios.

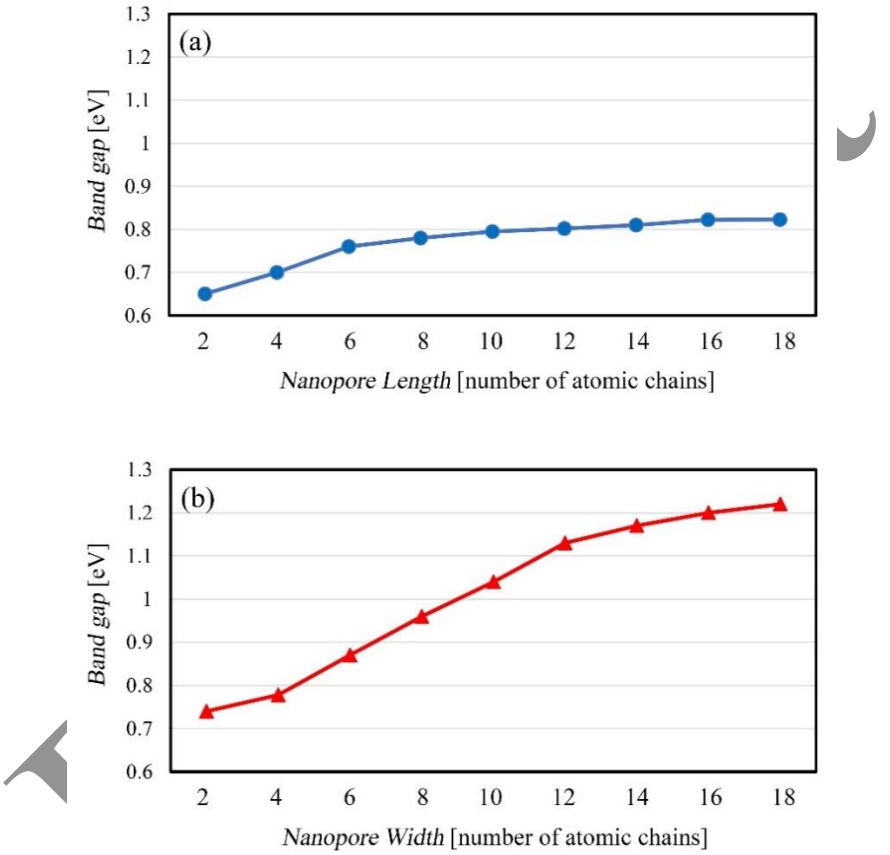

Fig. 4. Variation of the electronic energy band gap of zigzag bismuth nanoribbons with (a) nanopore length and (b) nanopore width, both measured in terms of the number of atomic chains.

Also, when the pore width increases, the upper and lower edges of the pore progressively approach the corresponding upper and lower boundaries of the nanoribbon. This geometric proximity plays a crucial role in modifying the interaction between the localized edge states formed around the pore and the

intrinsic edge states residing at the nanoribbon's outer boundaries. As the pore expands in the transverse direction, the vertical spacing between the pore's horizontal edges and the nanoribbon's outer edges diminishes considerably. This reduction in separation distance allows for enhanced overlap of the electronic wave functions associated with both the pore-induced localized states and the boundary edge states of the nanoribbon. As a result, the coupling and hybridization between these two distinct sets of edge states are substantially strengthened. This intensified interaction induces a more significant perturbation of the intrinsic edge transport channels.

Furthermore, Figure 4 presents the variation of the electronic band gap as a function of both nanopore length and width, expressed in terms of the number of atomic chains. Here, the band gap refers to the energy separation between the conduction and valence bands of the bulk-like states. As shown in panel (a), elongating the pore along the transport direction leads to a gradual increase in the band gap, which tends to saturate for sufficiently long pores. This trend originates from the enhanced localization of electronic states around the elongated pore boundaries. In contrast, panel (b) reveals that widening the pore in the transverse direction results in a more pronounced increase in the band gap. This behavior is attributed to the stronger confinement of carriers due to the geometric narrowing of the effective conduction channels. Therefore, while both pore elongation and widening contribute to the opening of an energy gap, the width variation plays a dominant role in modulating the electronic properties of the system.

As discussed earlier, the variation of nanopore length caused only moderate changes in the electrical conductance, while altering the pore width produced a much stronger effect on the transport characteristics. Therefore, in the following, we focus on the influence of pore width on the thermoelectric behavior, specifically on the Seebeck coefficient.

Previous studies have reported that a boxcar-shaped transmission or conductance spectrum is highly desirable for thermoelectric applications, as it can maximize the power factor and enhance the overall conversion efficiency. Interestingly, such a tendency toward a boxcar-like conductance profile is observed in zigzag bismuth nanoribbons with wider rectangular nanopores.

Figure 5 illustrates the variation of the Seebeck coefficient Sas a function of chemical potential for different pore widths. As the pore width increases, the conductance spectrum becomes closer to the ideal boxcar form, leading to a pronounced enhancement in the Seebeck coefficient. The results clearly show that the structure with a nanopore width of 14 atomic chains exhibits a Seebeck coefficient approximately four times larger than that of the ribbon with a width of 8 atomic chains. This remarkable improvement highlights the crucial role of

nanopore geometry in tuning the thermoelectric response of zigzag bismuth nanoribbons.

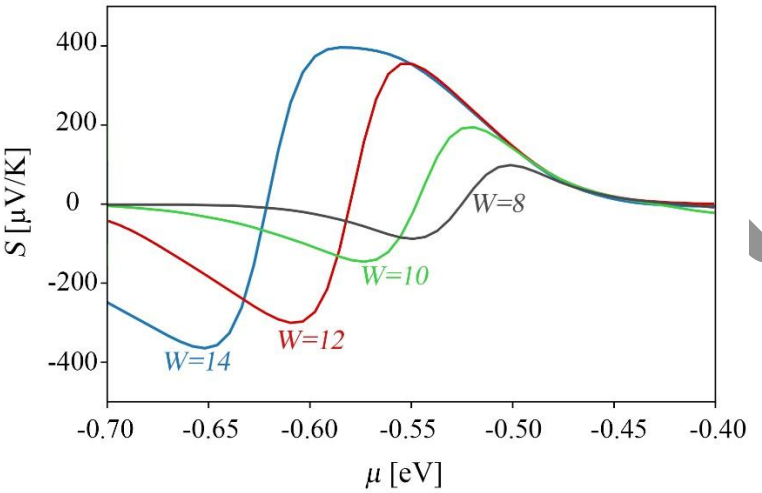

Fig. 5. Variation of the Seebeck coefficient (S) versus chemical potential (μ) for zigzag bismuth nanoribbons with rectangular nanopores of different widths (W = 8, 10, 12, and 14 atomic chains), showing the enhancement of (S) with increasing pore width.

6. CONCLUSION

In summary, we have examined how rectangular nanopores affect the electronic and thermoelectric properties of zigzag bismuth nanoribbons. We used a tight-binding approach along with Green's function methods. Our findings show that both the length and width of the nanopore significantly affect the transport characteristics of the nanoribbon. Lengthening the nanopore in the transport direction causes moderate scattering. This leads to a slight decrease in conductance and a gradual widening of the band gap between the conduction and valence bands of the bulk-like states. On the other hand, increasing the pore width in the direction perpendicular to transport results in a much stronger effect. It notably reduces conductance near the Fermi level and significantly increases the band gap. Additionally, our analysis of thermoelectric properties shows that the Seebeck coefficient improves greatly with greater pore width. This increase is linked to the conductance spectrum evolving toward a boxcar-like shape, which is known to boost thermoelectric performance. The nanoribbon featuring a nanopore width of 14 atomic chains has a Seebeck coefficient nearly four times

larger than that of a structure with a width of 8 atomic chains. Overall, these results underscore how sensitive zigzag bismuth nanoribbons are to geometric defects. Our findings also show that engineering nanopores is an effective way to adjust both the electronic and thermoelectric performance of bismuth-based low-dimensional materials for future nanoelectronics and energy-conversion applications.

ACKNOWLEDGMENT

Hossein Karbaschi and Mohammad Saiid Sobhan gratefully acknowledge the Mahallat Institute of Higher Education for its continuous support and commitment to academic excellence. Their dedication and resources played a vital role in the successful completion of this research.

References

1. H. Salehi, P. Amiri, R. Zare Hasanabad, *Ab-initio Study of Electronic, Optical, Dynamic and Thermoelectric Properties of $CuSbX_2$ (X=S, Se) Compounds.* Journal of Optoelectronical Nanostructures 3 (2) (2018) 53-64. Available: https://sanad.iau.ir/en/Article/1182780

2. T. Niazkar, G. Shams, and Z. Soltani, *Electronic, Optical, and Thermoelectric Properties of $BaFe_2xZn_xAs_2$ (x=0,1,2) orthorhombic Polymorphs: DFT Study*. Journal of Optoelectronical Nanostructures 6 (3) (2021) 93-116. Available: https://sanad.iau.ir/fa/Article/1182836.

3. H. Golamzadeh, R. Hosseini, H. Veladi, H. Rahimi, *Amplification of Output Voltage by Using Silicon Based Solar Cells, Piezoelectric and Thermoelectric Conversion Transducers: A Triple Energy Harvester.* Journal of Optoelectronical Nanostructures 8 (2) (2023) 32-50. Available: https://sanad.iau.ir/en/Article/1182931

4. S. Fotoohi, S. Haji Nasiri, *Vacancy Defects Induced Magnetism in Armchair Graphdiyne Nanoribbon.* Journal of Optoelectronical Nanostructures 4 (4) (2019) 15-38. Available: https://sanad.iau.ir/en/Article/1182808

5. M. Ghaedsharafi, M. R. Moslemi, F. Pesaran, *Defective HfS2 nanoribbons: the influence of vacancy defects and different atoms at the edge on this material with the first principle calculations.* Journal of Optoelectronical

Nanostructures 9 (1) (2024) 64-78. Available: https://sanad.iau.ir/en/Article/1182954

6. J. A. Ke, S. Garaj, S. Gradečak, *Nanopores in 2D MoS2: Defect-mediated formation and density modulation.* ACS Applied Materials & Interfaces, 11(29) (2019) 26228–26234. Available: https://pubs.acs.org/doi/10.1021/acsami.9b03531

7. H. Qiu, W. Zhou, W. Guo, *Nanopores in graphene and other 2D materials: a decade's journey toward sequencing.* ACS nano, 15(12) (2021) 18848–18864. Available: https://pubs.acs.org/doi/10.1021/acsnano.1c07960

8. M. Rezaei, H. Karbaschi, M. Amini, M. Soltani and G. Rashedi, *Thermoelectric properties of armchair phosphorene nanoribbons in the presence of vacancy-induced impurity band.* Nanotechnology, 32(37) (2021) 375704. Available: https://iopscience.iop.org/article/10.1088/1361-6528/ac08ba

9. S. Jalilvand, S. Sodagar, Z. Noorinejad, H. Karbaschi and M. Soltani, *The effect of vacancy induced localized states on the thermoelectric properties of armchair bilayer phosphorene nanoribbons*. Physica Scripta, 99(6) (2024) 0659c9. Available: https://iopscience.iop.org/article/10.1088/1402-4896/ad4ead

10. S. Sodagar, H. Karbaschi, M. Soltani, M. Amini, *Direct mapping of edge states in bilayer zigzag phosphorene nanoribbons into a SSH ladder model and optimizing their thermoelectric performance via edge state engineering.* The European Physical Journal Plus, 137(6) (2022) 722. Available: https://link.springer.com/article/10.1140/epjp/s13360-022-02942-x

11. J. Ou, Q. Zhang, *Enhanced Spin Thermopower in Phosphorene Nanoribbons via Edge-State Modifications.* Nanomaterials (Basel), 12(14) (2022) 2350. Available: https://www.mdpi.com/2079-4991/12/14/2350

12. H. Karbaschi, N. Nouri, M. Rezaie and G. Rashedi, *Thermoelectric power generation efficiency of zigzag monolayer nanoribbon of bismuth.* Nanotechnology, 31(37) (2020) 375403. Available: https://iopscience.iop.org/article/10.1088/1361-6528/ab946f

13. P. C. Lin, et al., *Doping graphene with substitutional Mn*. ACS nano, 15(3) (2021) 5449–5458. Available: https://pubs.acs.org/doi/10.1021/acsnano.1c00139

14. R. Singh, *Electronic and vibrational spectra of substitutional pair-defects of Boron and Nitrogen atoms in graphene and graphane.* Surface Science, 741 (2024) 122421. Available: https://www.sciencedirect.com/science/article/pii/S0039602823001747

15. H. Karbaschi, *Enhancing thermoelectric properties in zigzag bismuth nanoribbons via introduction of random impurities.* Journal of Nanoparticle Research, 27(8) (2025) 1–9. Available: https://link.springer.com/article/10.1007/s11051-025-06382-3

16. W. Ning, et al. *Robust surface state transport in thin bismuth nanoribbons*. scientific reports, (2014). Available: https://www.nature.com/articles/srep07086

17. Y. Li, et al. *In situ confined growth of bismuth nanoribbons with active and robust edge sites for boosted CO2 electroreduction.* ACS Energy Letters, 7(4) (2022) 1454–1461. Available: https://pubs.acs.org/doi/10.1021/acsenergylett.2c00326

18. I. I. Naumov, P. Dev, *Coexistence of quantum spin Hall and magnetic states in zigzag bismuth nanoribbons.* Applied Physics Letters, 123(9) (2023). Available: https://pubs.aip.org/aip/apl/article/123/9/093104/2908443/Coexistence-of-quantum-spin-Hall-and-magnetic

19. E. Aktürk, O.Ü. Aktürk, S. Ciraci, *Single and bilayer bismuthene: Stability at high temperature and mechanical and electronic properties.* Physical Review B, 94(1) (2016) 014115. Available: https://link.aps.org/doi/10.1103/PhysRevB.94.014115

20. R. R. Freitas, et al. *Topological insulating phases in two-dimensional bismuth-containing single layers preserved by hydrogenation.* The Journal of Physical Chemistry C, 119(41) (2015) 23599–23606. Available: https://pubs.acs.org/doi/10.1021/acs.jpcc.5b07961

21. Y. Liu, et al. *Strain-engineered conductivity transition and its mechanism in Bi (110) Film.* Surfaces and Interfaces, 56 (2025) 105595. Available: https://www.sciencedirect.com/science/article/pii/S2468023024017504

22. I. Bejenari, V. Kantser, A.A. Balandin, *Thermoelectric properties of electrically gated bismuth telluride nanowires.* Physical Review B, 81(7) (2010) 075316. Available: https://link.aps.org/doi/10.1103/PhysRevB.81.075316

23. J. Gou, et al. *Two-dimensional ferroelectricity in a single-element bismuth monolayer.* Nature, 617(7959) (2023) 67–72. Available: https://www.nature.com/articles/s41586-023-05848-5

24. L. Lv, et al. *Coordinating the edge defects of bismuth with sulfur for enhanced CO2 electroreduction to formate.* Angewandte Chemie, 135(25) (2023) e202303117. Available: https://onlinelibrary.wiley.com/doi/abs/10.1002/anie.202303117

25. M.R. Munna, M. Alam, *Bismuthene nanoribbon topological field-effect transistor: a DFT-NEGF-based study.* New Journal of Physics, 27(7) (2025) 073505. Available: https://iopscience.iop.org/article/10.1088/1367-2630/adf13f

26. Y. Liu, R.E. Allen, *Electronic structure of the semimetals Bi and Sb.* Physical Review B, 52(3) (1995) 1566. Available: https://link.aps.org/doi/10.1103/PhysRevB.52.1566

27. S. Sodagar, H. Karbaschi, M.Soltani and M.Amini, *Multidirectional strain-induced thermoelectric figure of merit enhancement of zigzag bilayer phosphorene nanoribbons.* Physica Scripta, 98(1) (2022) 015001. Available: https://iopscience.iop.org/article/10.1088/1402-4896/aca440

28. C.W. Groth, et al. *Kwant: a software package for quantum transport.* New Journal of Physics, 16(6) (2014) 063065. Available: https://iopscience.iop.org/article/10.1088/1367-2630/16/6/063065/meta